Electronic Supplementary Material (ESI) for New Journal of Chemistry.

Supporting Information for

An iron-based metal-organic framework for selective CO_2 adsorption and efficient anode material for lithium-ion battery

Y B. N. Tran,[ab] Phuong T. K. Nguyen,[*ab] and Tuan Loi Nguyen[ab]

[a]Institute of Fundamental and Applied Sciences, Duy Tan University, Ho Chi Minh City 700000, Viet Nam

[b]Faculty of Natural Sciences, Duy Tan University, Da Nang, 550000, Viet Nam.

*To whom correspondence should be addressed: Email, nguyentkieuphuong1@duytan.edu.vn.

Table of Contents

Section S1: Materials and Analytical Techniques

Chemicals and Materials

Copper(I) iodide (CuI, ≥ 99.5%), 1,8-diazabicylcloundec-7-ene (DBU, ≥ 99.0%), sodium hydroxide (NaOH, reagent grade, ≥ 98%), trimesic acid (H_3BTC, 95%), iron (III) acetylacetonate ($Fe(acac)_3$, ≥99.9%), iron (III) nitrate nonahydrate ($Fe(NO_3)_3 \cdot 9H_2O$, ≥99.9%), poly(vinylidene fluoride) **(**PVDF, average Mw ~534,000 by GPC), lithium hexafluorophosphate solution ($LiPF_6$, 1 M, in ethylene carbonate (EC) : diethyl carbonate (DEC) = 1:1, v/v), Celgard 2400, and hydrochloric acid (HCl, 1 M) were obtained from Sigma-Aldrich. Methyl-4-iodobenzoate (98%), bis(tripheny-phosphine)palladium(II) chloride ($PdCl_2(PPh_3)_2$, 98%), diethylamine (DEA, 99.5%), trimethylsilylacetylene (98%), dicobalt octacarbonyl ($Co_2(CO)_8$, 95%), anhydrous 1,4-dioxane (99.8%), anhydrous tetrahydrofuran (THF, 99.85%), anhydrous methanol (MeOH, 99.5%), and *N,N*-dimethylformamide (DMF, 99.8%) were purchased from Acros Organics. Anhydrous dichloromethane (DCM), ammonium chloride (99.998%), anhydrous sodium sulfate, *N*-methyl-2-pyrrolidone (NMP, 99.5%), and glacial acetic acid (CH_3COOH, ≥99.85%) were obtained from Merck Chemical Co. Carbon black Super P (99+) was obtained from Alfa Aesar. Copper foil (thickness 12 μm, >99.9%) and lithium foil (thickness 0.1 mm, >99.9%) were purchased from Tob New Energy Company. Diethylamine and deionized water (ultrapure, 17.8 MΩ·cm resistivity, obtained from a Barnstead Easypure II system) were degassed with a stream of N_2 for 5 min prior to addition into the Sonogashira coupling reactions. All other chemicals were used without further purification unless otherwise noted.

Synthesis of Fe-MIL-100. Fe-MIL-100 was synthesized following previous works with slight modifications.[S1,S2] $Fe(NO_3)_3 \cdot 9H_2O$ (3.26 g, 9.2 mmol) and trimesic acid (1.13 g, 5.4 mmol) were dissolved in 40 mL water. The reactant mixture was stirred at room temperature for 1h and accordingly loaded in a Teflon-lined pressure vessel. The reactor vessel was heated up to 160°C for 12h to produce a light orange solid. The solid was filtrated, washed with deionized water (3 × 10 mL), and treated in hot deionized water (10 mL, ~80°C) for 3h to eliminate the residuals iron salt and H_3BTC linker. The MOF solid was then dried at room temperature for 18 h, followed by heating at 80 °C under vacuum for an additional 24 h.

Analytical Techniques

Optical microscope images were collected on Nikon SMZ1000 Zoom Stereomicroscope. Elemental microanalyses (EA) were performed on a LECO CHNS-932 Analyzer. Thermal gravimetric analysis (TGA) was performed on a TA Q500 thermal analysis system with the sample held in a platinum pan in a continuous airflow. Field-emission Scanning Electron Microscope (FE-SEM) was performed on an ultralow voltage imaging with Hitachi's S-4800 FE-SEM operating at an accelerating voltage of 1 kV. Energy dispersive X-ray analyzer (EDX) was conducted on a Horiba H-7593.

Section S2: Characterizations, Powder X-Ray Diffraction and Structural Refinement of Fe-CPB

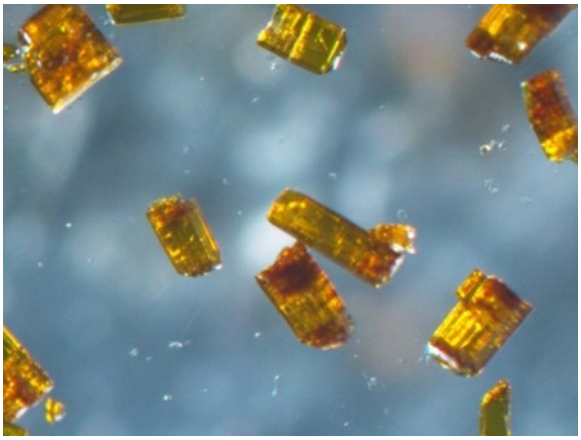

Figure S1. Optical microscope image of Fe-CPB.

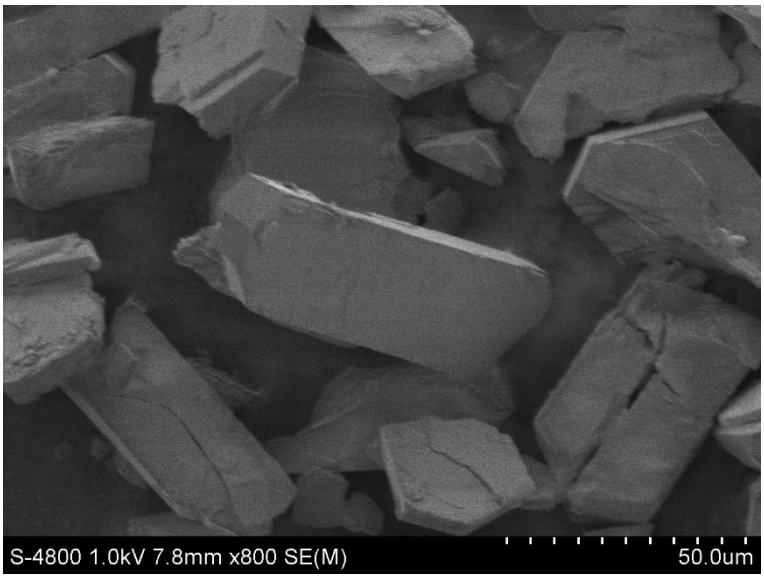

Figure S2. SEM image of Fe-CPB.

Table S1. Unit cell parameters and fractional atomic coordinates for the refined crystal Fe-CPB.

Empirical formula, Space group		$C_{64}H_{58}Fe_4N_4O_{20}$, *P*2/*c*			
Refined unit cell		*a* = 28.1854 Å, *b* = 15.6499 Å, *c* = 13.5063 Å, α = γ = 90.0000°, β = 98.8648°.			
Pawley refinement		R_{wp} = 3.70%, R_{wp} (w/o background) = 4.48%, R_p = 1.82%			
Atom label	Atom type	*x*	*y*	*z*	Site Occupancy
Fe3	Fe	0.32852	-0.03371	0.5913	1
Fe4	Fe	0.34647	-0.06143	0.84129	1
Fe1	Fe	0.17428	0.45889	0.8682	1
Fe2	Fe	0.17131	0.47138	0.61962	1
O19	O	0.32	0.05124	0.47024	1
O13	O	0.3556	0.90351	0.71015	1
O2	O	0.15449	1.41183	0.73616	1
C50	C	0.00155	0.56292	0.93208	1
H50A	H	-0.01507	0.58593	0.87052	1
H50B	H	0.02142	0.60646	0.96737	1
H50C	H	-0.02134	0.54347	0.97283	1
O9	O	0.19178	0.546	0.98781	1
O11	O	0.24509	0.4617	0.8364	1
O12	O	0.23646	0.51931	0.68359	1
O15	O	0.37514	0.05827	0.8302	1
O3	O	0.25854	1.00681	0.61804	1
O16	O	0.36794	0.06515	0.66448	1
O5	O	0.13265	0.58154	0.62683	1
O14	O	0.4013	0.92085	0.59456	1
O4	O	0.27666	1.00503	0.78309	1
O1	O	0.10712	1.41798	0.59246	1
O8	O	0.19285	0.35426	0.96261	1
O17	O	0.41667	-0.09579	0.91548	1

O6	O	0.14231	0.56443	0.79071	1
O18	O	0.3074	-0.13647	0.49577	1
O20	O	0.3162	0.17216	0.39055	1
O10	O	0.20969	0.6623	1.07273	1
O7	O	0.10329	0.43836	0.90446	1
C32	C	0.46747	0.4856	0.76893	1
C47	C	0.38178	0.09308	0.75058	1
C45	C	0.40976	0.17594	0.75763	1
C29	C	0.41404	0.4858	0.76548	1
C33	C	0.49226	0.56297	0.77008	1
C9	C	0.04689	0.99521	0.75295	1
C5	C	0.04724	1.15544	0.74479	1
C40	C	0.39045	0.87949	0.66576	1
C26	C	0.31477	0.48921	0.76346	1
C41	C	0.49248	0.40759	0.77287	1
C42	C	0.46441	0.32599	0.7681	1
C34	C	0.46534	0.64543	0.74888	1
C8	C	0.02332	1.07272	0.76326	1
C37	C	0.41585	0.7978	0.69698	1
C21	C	0.09992	0.68589	0.72529	1
C18	C	0.04907	0.83546	0.75047	1
C16	C	0.2478	1.00476	0.7039	1
N1	N	0.47569	-0.08756	1.04811	1
C17	C	0.02346	0.9177	0.76368	1
C36	C	0.41195	0.75735	0.78635	1
H36	H	0.39266	0.78077	0.82943	1
C49	C	0.00693	0.41042	0.8828	1
H49A	H	0.02419	0.37952	0.8383	1
H49B	H	-0.02517	0.4214	0.85	1
H49C	H	0.00585	0.37708	0.9421	1
C25	C	0.26116	0.48957	0.76125	1

C13	C	0.19534	1.00245	0.7143	1
C35	C	0.43668	0.682	0.8121	1
H35	H	0.43401	0.6556	0.87273	1
C10	C	0.09838	0.99616	0.73676	1
C2	C	0.09361	1.30536	0.70214	1
C7	C	0.10364	1.26839	0.79566	1
H7	H	0.12587	1.29373	0.84501	1
C24	C	0.12696	0.6043	0.7127	1
C27	C	0.34564	0.4781	0.85202	1
H27	H	0.33337	0.47191	0.91169	1
C43	C	0.44144	0.29571	0.67737	1
H43	H	0.44397	0.32575	0.61903	1
C01I	C	0.30704	0.12962	0.46268	1
C31	C	0.33357	0.49877	0.67595	1
H31	H	0.31313	0.50633	0.61561	1
C30	C	0.38323	0.49733	0.67723	1
H30	H	0.39557	0.50412	0.61775	1
C6	C	0.08079	1.1939	0.81651	1
H6	H	0.08808	1.16924	0.87963	1
C39	C	0.46799	0.68547	0.65837	1
H39	H	0.4865	0.6613	0.61436	1
C22	C	0.08031	0.73327	0.64314	1
H22	H	0.08378	0.71514	0.57911	1
C12	C	0.1819	0.98251	0.80542	1
H12	H	0.20538	0.97158	0.86028	1
C23	C	0.05543	0.80793	0.65573	1
H23	H	0.0428	0.83999	0.59989	1
C44	C	0.41456	0.22096	0.67187	1
H44	H	0.39969	0.20109	0.60991	1
C46	C	0.43173	0.20677	0.84857	1
H46	H	0.42829	0.17766	0.90712	1

C1	C	0.11913	1.38313	0.6753	1
C28	C	0.395	0.47609	0.85278	1
H28	H	0.41543	0.46807	0.91307	1
C56	C	0.43386	-0.06405	0.99684	1
H56	H	0.41655	-0.02146	1.02343	1
C62	C	0.45902	0.28105	0.85385	1
H62	H	0.47385	0.30082	0.91594	1
C14	C	0.15997	1.01896	0.6342	1
H14	H	0.16846	1.03196	0.57206	1
C38	C	0.44369	0.76031	0.63273	1
H38	H	0.44594	0.78612	0.57163	1
C11	C	0.13389	0.97849	0.81634	1
H11	H	0.12549	0.96363	0.87799	1
N2	N	0.27313	-0.2012	0.3554	1
C19	C	0.06856	0.78748	0.8319	1
H19	H	0.06469	0.80491	0.89601	1
C15	C	0.11178	1.01638	0.64512	1
H15	H	0.08834	1.02824	0.59056	1
C20	C	0.09404	0.71304	0.81942	1
H20	H	0.10719	0.68141	0.87521	1
C54	C	0.21125	0.62058	0.99628	1
C3	C	0.05961	1.26764	0.63083	1
H3	H	0.05219	1.29224	0.56761	1
N3	N	0.23068	0.29315	1.10271	1
C4	C	0.03666	1.19405	0.65251	1
H4	H	0.01357	1.16992	0.60397	1
C59	C	0.27771	-0.14024	0.42081	1
H59	H	0.25618	-0.09497	0.40921	1
C028	C	0.27988	0.16845	0.53881	1
H02A	H	0.25065	0.13727	0.53993	1
H02B	H	0.27244	0.22697	0.52143	1

H02C	H	0.29922	0.16608	0.60383	1
C51	C	0.22451	0.35266	1.03596	1
H51	H	0.2459	0.39824	1.04412	1
C58	C	0.49308	-0.05313	1.14721	1
H58A	H	0.4716	-0.00928	1.16289	1
H58B	H	0.52453	-0.02931	1.14794	1
H58C	H	0.49458	-0.09798	1.19602	1
C57	C	0.50412	-0.15239	1.00846	1
H57A	H	0.50445	-0.20332	1.04823	1
H57B	H	0.53637	-0.13202	1.0104	1
H57C	H	0.49041	-0.16493	0.94049	1
C55	C	0.23604	0.65621	0.91488	1
H55A	H	0.26865	0.63633	0.92375	1
H55B	H	0.23572	0.71748	0.91779	1
H55C	H	0.21965	0.63762	0.85088	1
C48	C	0.07763	0.49115	0.92252	1
H48	H	0.09242	0.54078	0.94985	1
C61	C	0.23356	-0.20305	0.27107	1
H61A	H	0.21165	-0.15715	0.27789	1
H61B	H	0.21688	-0.2566	0.27071	1
H61C	H	0.2461	-0.19659	0.20934	1
C52	C	0.19807	0.22282	1.09649	1
H52A	H	0.17221	0.23225	1.04239	1
H52B	H	0.18535	0.21794	1.15825	1
H52C	H	0.21461	0.17116	1.08464	1
C60	C	0.30621	-0.26833	0.36421	1
H60A	H	0.33343	-0.254	0.41335	1
H60B	H	0.31668	-0.27791	0.30067	1
H60C	H	0.29141	-0.31932	0.38449	1
C53	C	0.27123	0.29356	1.18437	1

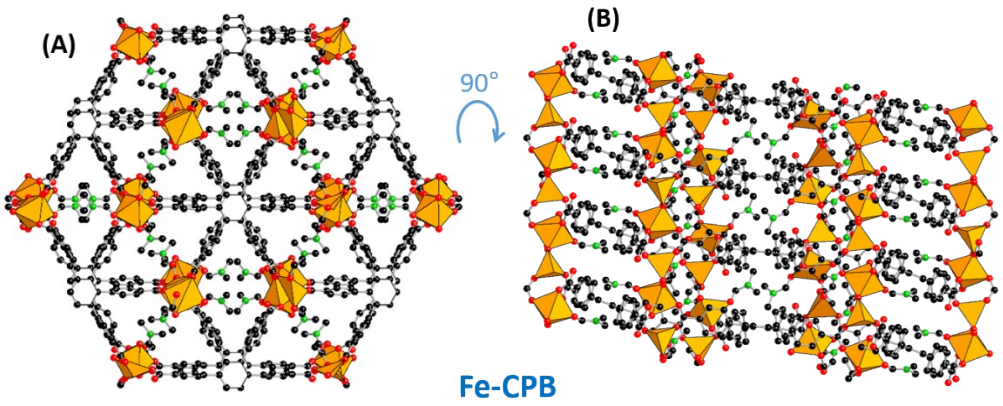

Figure S3. Crystal structure of as-synthesized Fe-CPB with the presence of coordinated DMF. Color code: Fe, orange polyhedra; C, black; O, red; N. green. All H atoms are omitted for clarity.

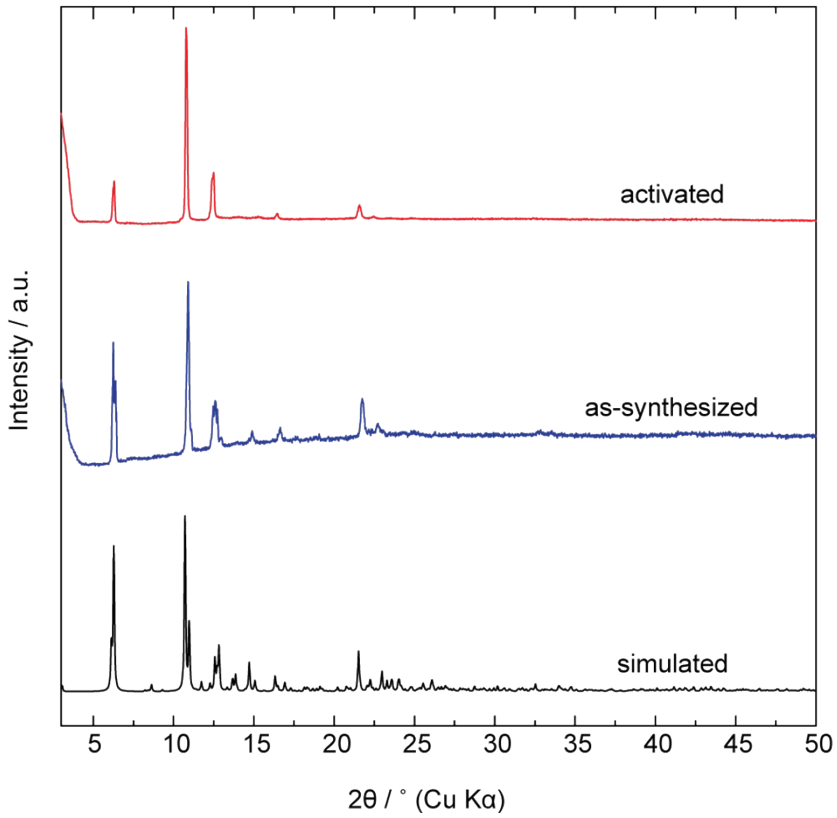

Figure S4. Comparison of the simulated (black) PXRD pattern from the single crystal data with the experimental as-synthesized (blue) and activated (red) PXRD patterns of Fe-CPB.

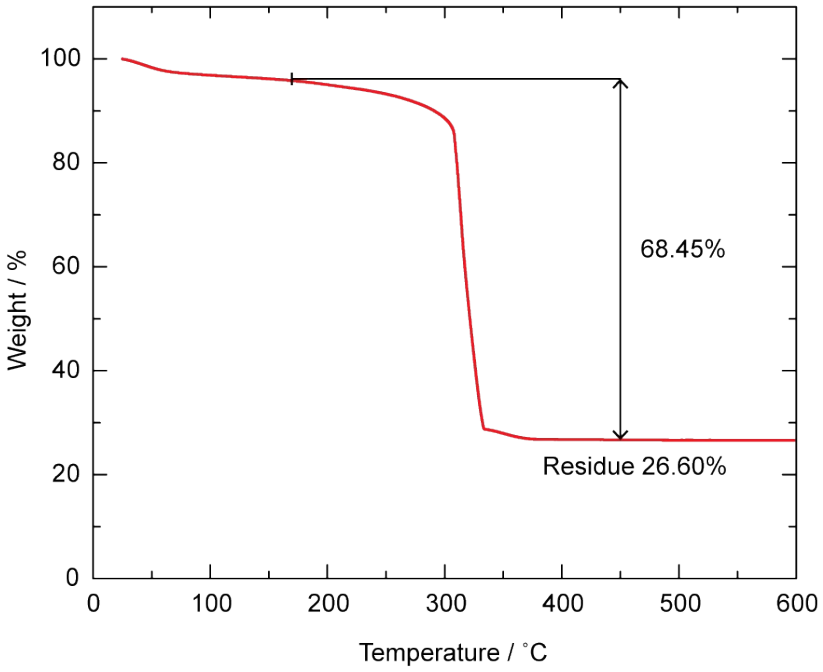

Figure S5. TGA traces of activated Fe-CPB at a heating rate of 5 °C min^{-1} under air flow.

Section S3: Gas Adsorption Studies of Fe-CPB

Gas selectivity calculated by Henry's Law

Virial-type equation was employed for estimation of Henry's constant:

$$\ln P = \ln N + \frac{1}{T}\sum_{i=0}^{m} a_i N^i + \sum_{i=0}^{n} b_i N^i$$

Where P is pressure, N is the adsorbed amount, T is temperature, a_i and b_i are virial coefficient, and m and n are the number of virial coefficients required for adequate fitting of the isotherms. As a result, Henry's constant (K_H) at the temperature T can be calculated:

$$K_H = \exp(-b_0) \cdot \exp(-a_0/T)$$

The Henry's Law selectivity for gas component i over j is calculated:

$$S_{ij} = K_{Hi}/K_{Hj}$$

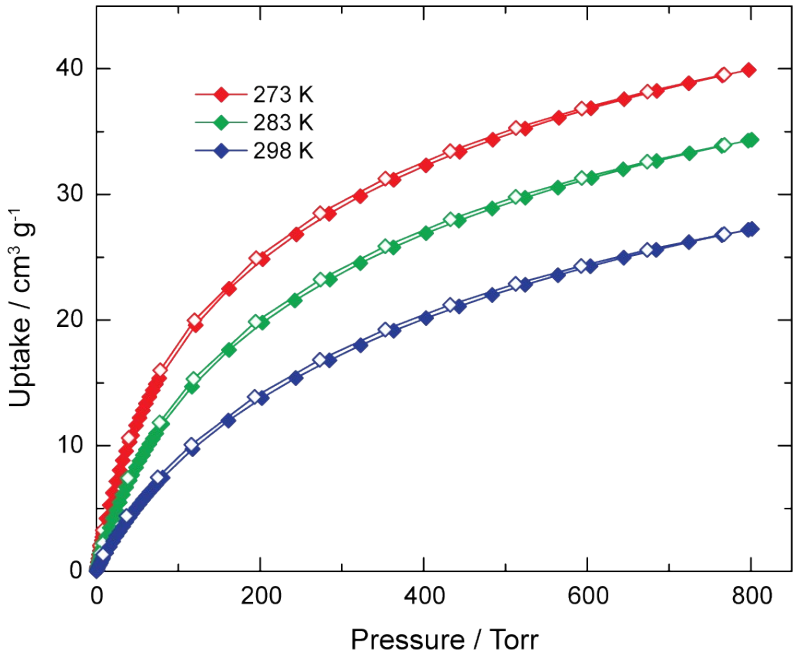

Figure S6. CO_2 isotherms for Fe-CPB at 273 (red), 283 (green), and 298 K (blue). Filled and open symbols represent adsorption and desorption branches, respectively. The connecting curves are guides for the eye.

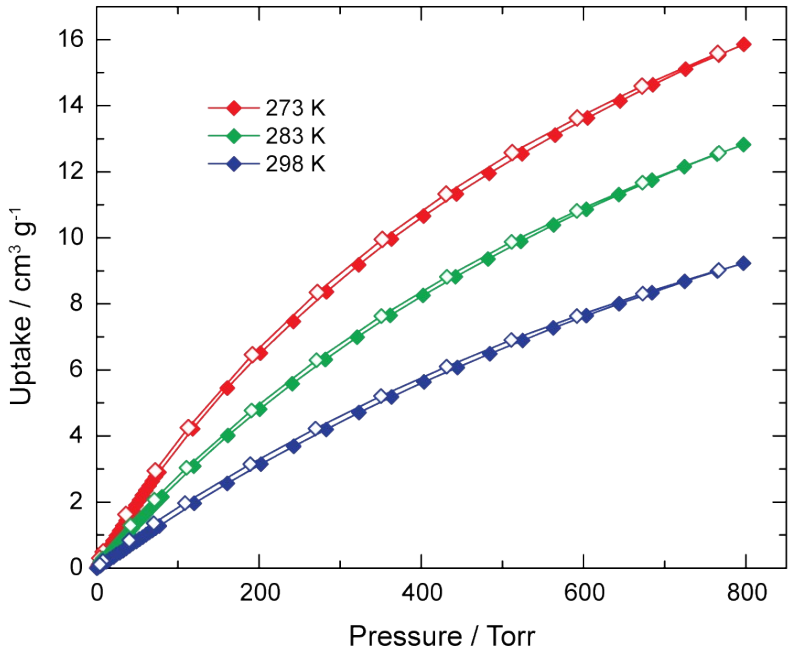

Figure S7. CH_4 isotherms for Fe-CPB at 273 (red), 283 (green), and 298 K (blue). Filled and open symbols represent adsorption and desorption branches, respectively. The connecting curves are guides for the eye.

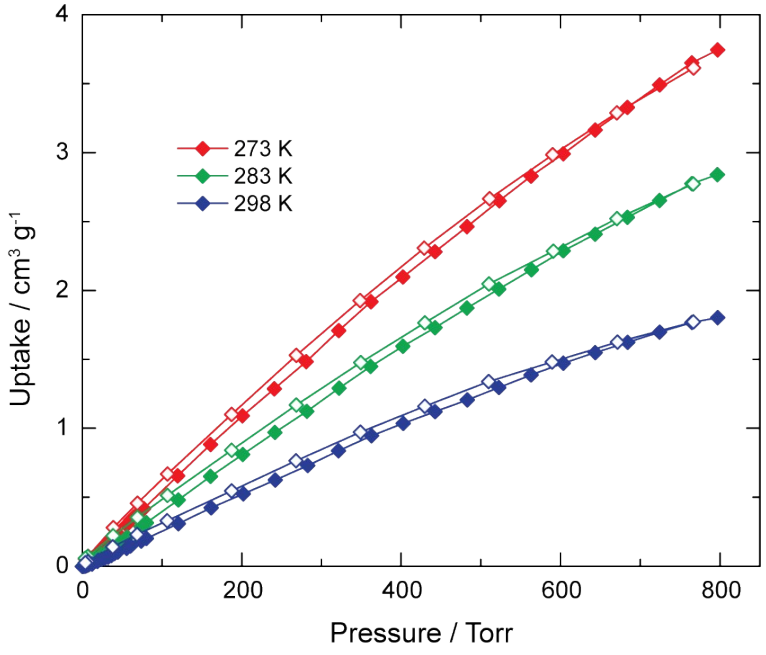

Figure S8. N_2 isotherms for Fe-CPB at 273 (red), 283 (green), and 298 K (blue). Filled and open symbols represent adsorption and desorption branches, respectively. The connecting curves are guides for the eye.

Section S4: Electrochemical Studies of Fe-CPB

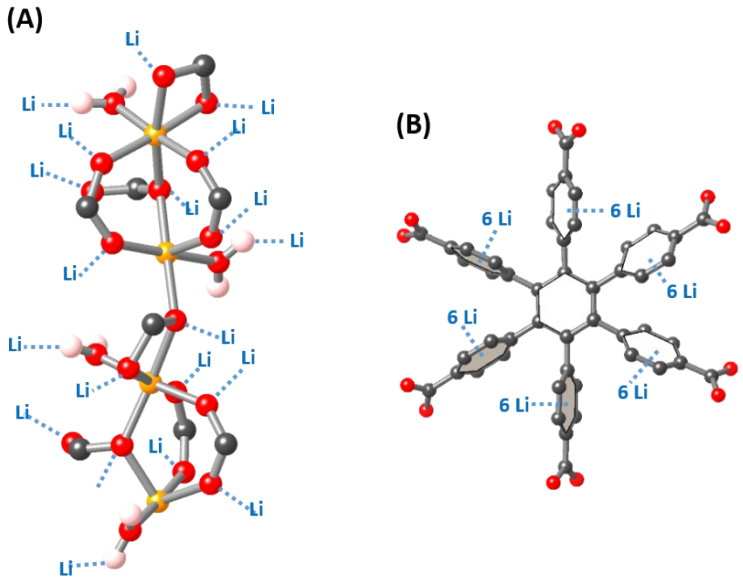

Figure S9. Possible sites for Li^+ insertion at (A) the iron-oxo cluster and (B) the organic CPB linker of Fe-CPB.

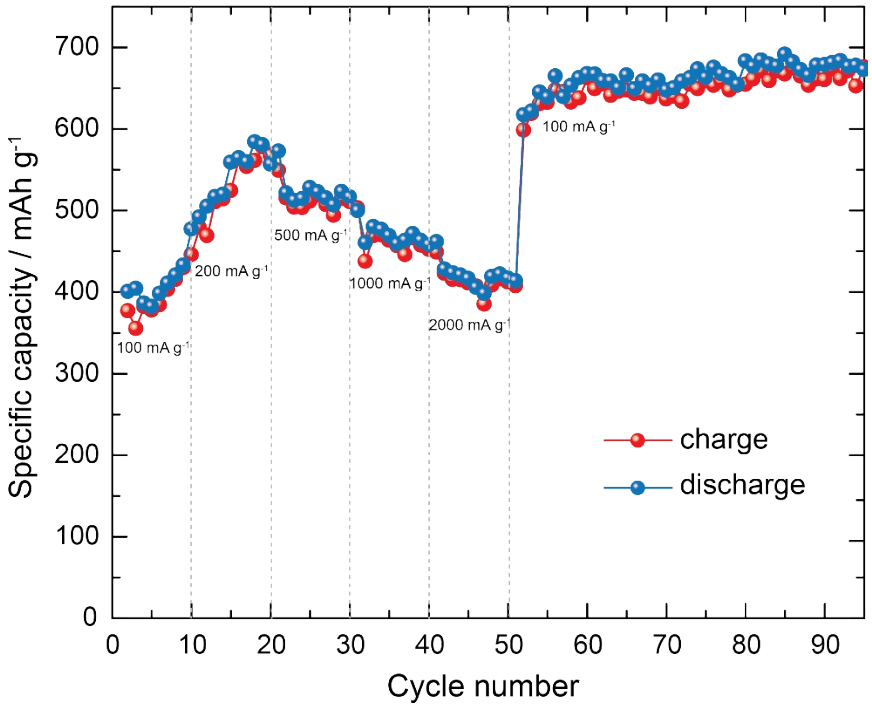

Figure S10. Rate capability of Fe-CPB at different current densities

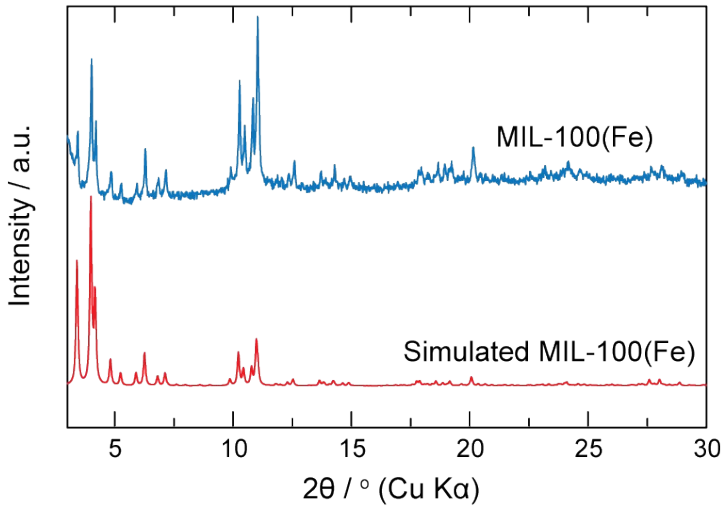

Figure S11. Comparison of the simulated (black) PXRD pattern from the reported structure data with the experimental activated (blue) PXRD of Fe-MIL-100.

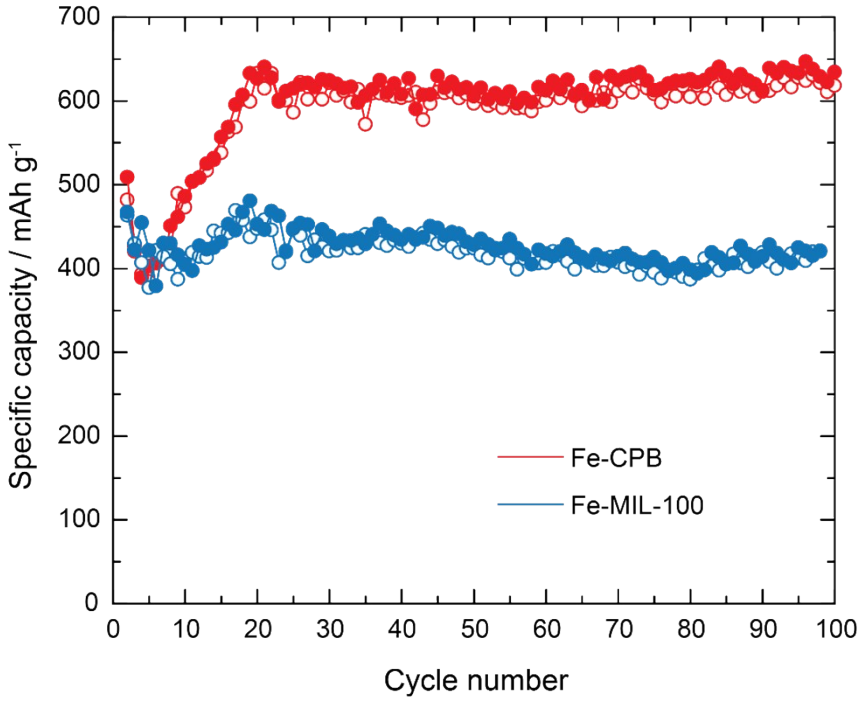

Figure S12. The cycling performance of Fe-CPB and Fe-MIL-100 at the current density of 100 mA g^{-1}. Filled and open symbols represent discharge and charge processes, respectively.

Table S2. Comparison of pristine MOFs as anodic materials for lithium-ion batteries.

#	MOF (wt%)	Capacity/ mAh g^{-1}	Current density/ mA g^{-1}	Cycle number	Capacity/mAh g^{-1} @ Highest current/mA g^{-1}	Ref.
1	Fe-CPB (60 wt%)	634	100	100	416@ 2000	This work
2	Fe-MIL-88B (60 wt%)	744.5	60	400	~200@2 000	[S3]
3	Mn-BTC (70 wt%)	600	103	100	250@ 2061	[S4]
4	Pb-BTC (80%)	625	100	150	190@ 2000	[S5]
5	Co-L1 (80 wt%)	617	100	200	346@ 1000	[S6]
6	Li-MOF (60 wt%)	458	100	80	-	[S7]
7	$Zn_3(HCOO)_6$ (70 wt%)	560	60	60	265@ 3000	[S8]
8	$Zn(Im)_{1.5}(abIm)_{0.5}$ (70 wt%)	~190	100	200	75@ 400	[S9]

Section S5: Post-Cycling Characterizations of Fe-CPB

The ethylene carbonate solvent reduction reaction proceeds as follows:

$(CH_2O)_2CO + e^- \rightarrow [(CH_2O)_2CO]^-$

$2[(CH_2O)_2CO]^- \rightarrow C_2H_4 + CH_2(OCO_2)^-CH_2(OCO_2)^-$

$CH_2(OCO_2)^-CH_2(OCO_2)^- + 2\ Li^+ \rightarrow CH_2(OCO_2)LiCH_2(OCO_2)Li$

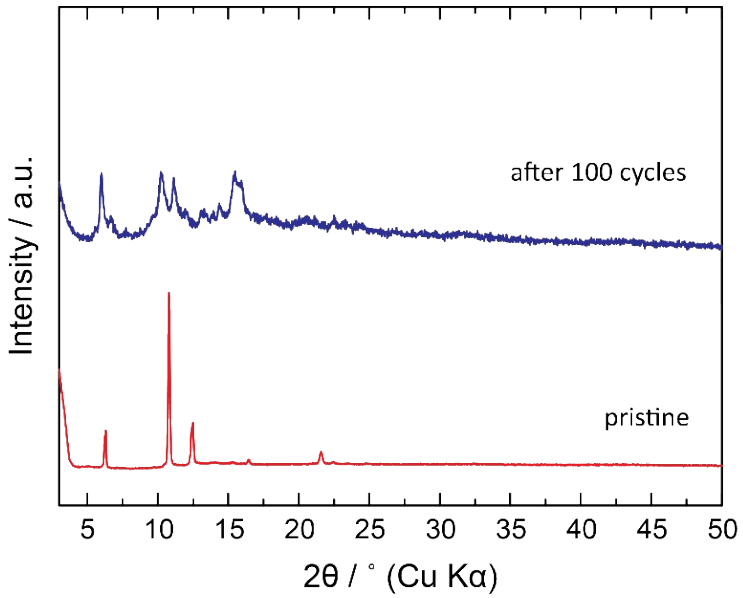

Figure S13. PXRD of pristine Fe-CPB and cycled Fe-CPB electrode after 100 cycles.

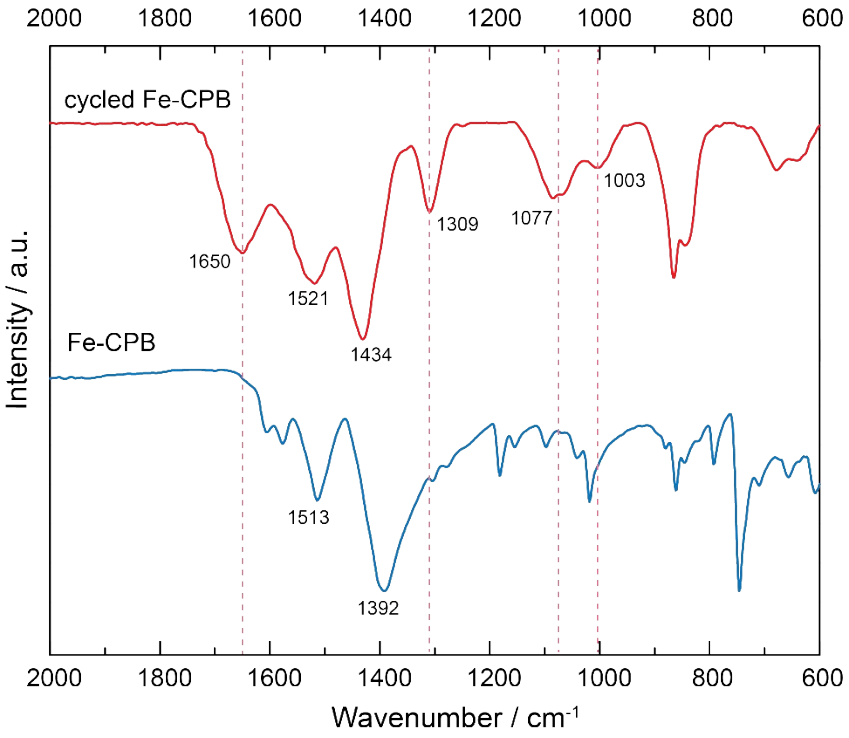

Figure S14. FTIR of pristine Fe-CPB and cycled Fe-CPB electrode after 100 cycles.

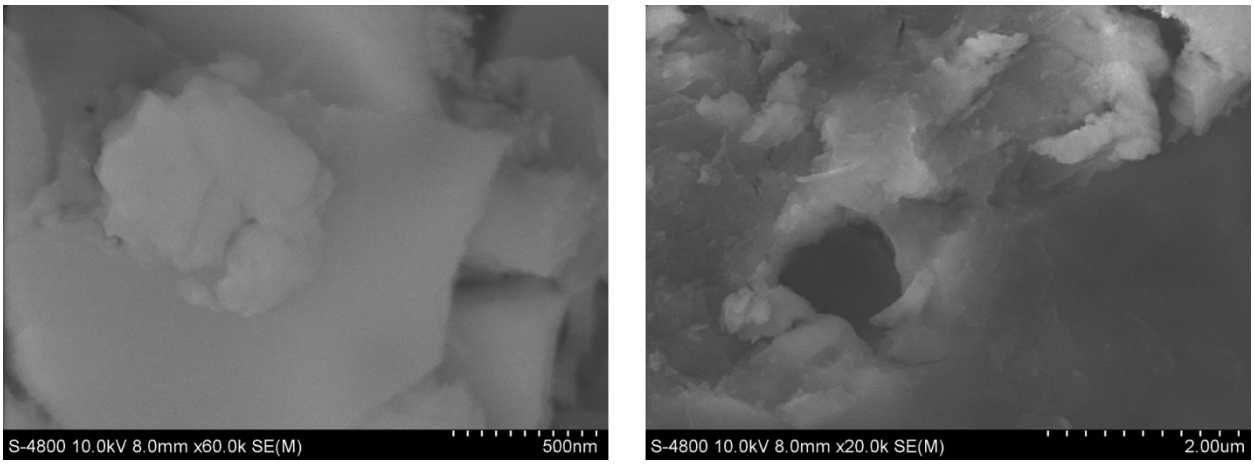

Figure S15. SEM images of cycled Fe-CPB electrode after 100 cycles.

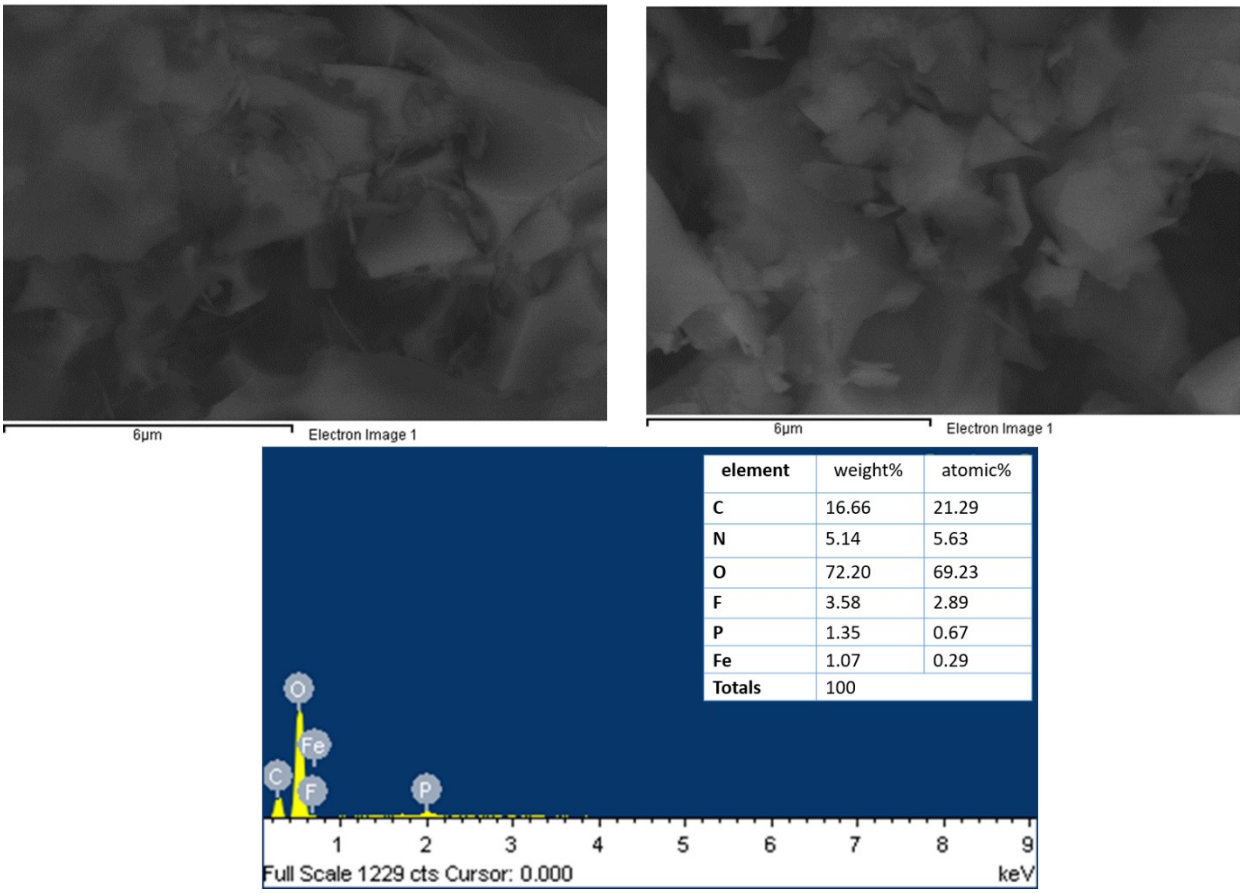

Figure S16. SEM-EDX analysis of recycled Fe-CPB electrode after 100 cycles

Section S6: References

[S1] P. Horcajada, S. Surblé, C. Serre, D.-Y. Hong, Y.-K. Seo, J.-S. Chang, J.-M. Grenèche, I. Margiolaki and G. Férey, *Chem. Commun.*, 2007, 2820-2822.

[S2] Y.-K. Seo, J. W. Yoon, J. S. Lee, U. H. Lee, Y. K. Hwang, C.-H. Jun, P. Horcajada, C. Serre and J.-S. Chang, *Microporous Mesoporous Mater.*, 2012, **157**, 137-145.

[S3] L. Shen, H. Song and C. Wang, *Electrochim. Acta*, 2017, **235**, 595-603.

[S4] S. Maiti, A. Pramanik, U. Manju and S. Mahanty, *ACS Appl. Mater. Interfaces*, 2015, **7**, 16357-16363.

[S5] F. Baskoro, H. Q. Wong, K. B. Labasan, C.-W. Cho, C.-W. Pao, P.-Y. Yang, C.-C. Chang, C.-I. Chen, C.-C. Chueh, W. Nie, H. Tsai and H.-J. Yen, *Energy Fuels*, 2021, **35**, 9669-9682.

[S6] T. Gong, X. Lou, E.-Q. Gao and B. Hu, *ACS Appl. Mater. Interfaces*, 2017, **9**, 21839-21847.

[S7] X. Han, F. Yi, T. Sun and J. Sun, *Electrochem. Commun.*, 2012, **25**, 136-139.

[S8] K. Saravanan, M. Nagarathinam, P. Balaya and J. J. Vittal, *J. Mater. Chem.*, 2010, **20**, 8329-8335.

[S9] Y. Lin, Q. Zhang, C. Zhao, H. Li, C. Kong, C. Shen and L. Chen, *Chem. Commun.*, 2015, **51**, 697-699.